

# Highly Efficient Non-relativistic Edelstein effect in $p$ -wave magnets

Atasi Chakraborty,<sup>1,\*</sup> Anna Birk Hellenes,<sup>1</sup> Rodrigo Jaeschke-Ubiergo,<sup>1</sup>  
Tomás Jungwirth,<sup>2,3</sup> Libor Šmejkal,<sup>4,1,2</sup> and Jairo Sinova<sup>1,5,†</sup>

<sup>1</sup>*Institut für Physik, Johannes Gutenberg Universität Mainz, D-55099 Mainz, Germany*

<sup>2</sup>*Institute of Physics, Academy of Sciences of the Czech Republic,  
Cukrovarnická 10, 162 00 Praha 6, Czech Republic*

<sup>3</sup>*School of Physics and Astronomy, University of Nottingham, NG7 2RD, Nottingham, United Kingdom*

<sup>4</sup>*Max Planck Institute for the Physics of Complex Systems, Nöthnitzer Str. 38, 01187 Dresden, Germany*

<sup>5</sup>*Department of Physics, Texas A & M University, College Station, Texas 77843-4242, USA*

The origin and efficiency of charge-to-spin conversion, known as the Edelstein effect (EE), has been typically linked to spin-orbit coupling mechanisms, which require materials with heavy elements within a non-centrosymmetric environment. Here we demonstrate that the high efficiency of spin-charge conversion can be achieved even without spin-orbit coupling in the recently identified coplanar  $p$ -wave magnets. The non-relativistic Edelstein effect (NREE) in these magnets exhibits a distinct phenomenology compared to the relativistic EE, characterized by a strongly anisotropic response and an out-of-plane polarized spin density resulting from the spin symmetries. We illustrate the NREE through minimal tight-binding models, allowing a direct comparison to different systems. Through first-principles calculations, we further identify the  $p$ -wave candidate material CeNiAsO as a high-efficiency NREE material, revealing a 25 times larger response than the maximally achieved relativistic EE and other reported NREE in non-collinear magnetic systems with broken time-reversal symmetry. This highlights the potential for efficient spin-charge conversion in  $p$ -wave magnetic systems.

Conventional spintronics [1, 2] typically relies on ferromagnetic materials and external magnetic fields to generate spin-polarized charge currents. More recent spintronic device concepts focus on effects generating spin-current or spin-density accumulation by electric fields [3, 4]. The latter is known as the Edelstein effect (EE), appearing in non-centrosymmetric materials and usually originating from relativistic (spin-orbit coupling) effects, as illustrated in Fig. 1a and 1b [5–7]. Archetypal applications of the EE include spin-orbit torque devices, such as the magneto-electric spin-orbit (MESO) transistor [4, 8–10], where efficient charge-to-spin conversion is required to exert a torque that can switch the magnetization orientation [11–17]. The relativistic EE has been demonstrated in numerous systems including Rashba-Dresselhaus systems [18, 19], topological insulators [20], semiconductors [21, 22], Weyl semimetals [23, 24], oxide interfaces [25–27], 2D electron gases [28, 29] and non-centrosymmetric superconductors [30]. The non-equilibrium spin density in these systems originates from spin-orbit coupling (SOC), necessitating heavy elements to reach functional efficiencies of charge-to-spin conversion [26].

The possibility of a non-relativistic EE (NREE) was proposed recently in non-collinear magnetic systems with broken time-reversal symmetry (TRS) band structure and broken parity [31–34], allowing for a current-induced spin accumulation in systems also with possibly light elements. However, these magnetic systems do not fully mimic the relativistic EE, since they break TRS in momentum space. The recently predicted  $p$ -wave magnets (Fig. 1c), which preserve TRS in momentum space [35], provide a direct non-relativistic analog to the relativistic

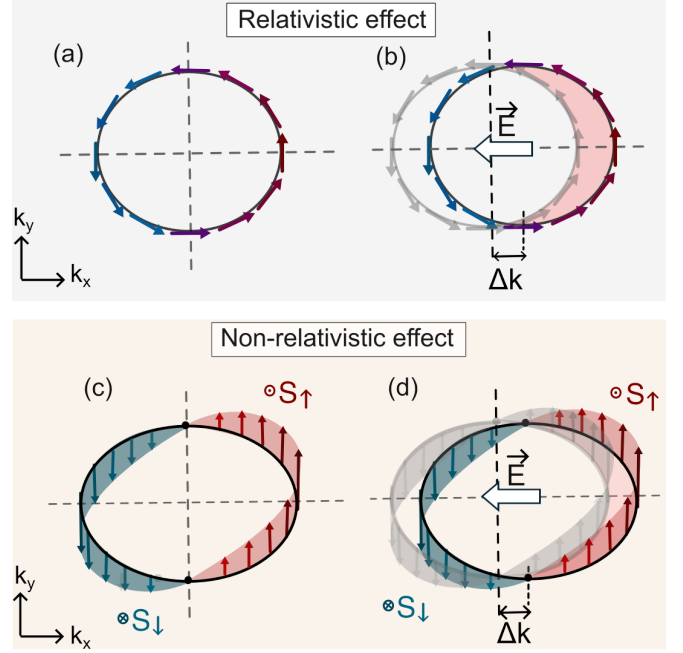


FIG. 1. (a) Schematic of a relativistic Rashba spin-texture (1 band). (b) (Relativistic Edelstein effect) Non-equilibrium redistribution resulting in a net in-plane spin-accumulation. (c) Schematic of non-relativistic out-of-plane spin polarization texture of  $p$ -wave magnets originating from non-collinear  $\mathcal{T}\bar{t}$  co-planar magnetic order. (d) (Non-relativistic Edelstein effect) Non-equilibrium out-of-plane spin-accumulation driven by an external electric field.

EE.

The prediction and the identification of the favorable characteristics for high NREE efficiency of  $p$ -wave magnetic candidates were made possible by applying the spin

symmetries approach, instrumental in the discovery of altermagnets [36]. Using the spin symmetries to fully classify and delimit all collinear spin arrangements on crystals leads to the conclusion that only even-parity non-relativistic spin-split band structures (s-, d-, g-, or i-wave) are possible in collinear magnetic systems [36, 37]. This narrows the search for  $p$ -wave (and higher odd-parity) magnets to non-collinear systems [35]. A  $p$ -wave magnet must break both parity ( $P$ ) and  $P\mathcal{T}$  symmetry, and preserve  $\mathcal{T}\vec{t}$  symmetry, where  $\vec{t}$  is a translation. This last symmetry preserves TRS in momentum space and enforces zero net magnetization.  $P$ -wave magnetic candidates with collinear polarized band structure have been identified in the co-planar magnets, which have the spin symmetry  $[C_{2\perp}||\vec{t}]$ , where  $C_{2\perp}$  being a  $180^\circ$  spin rotation along the axis perpendicular to the spins [35]. This spin symmetry mandates that the spin polarization axis in the electronic structure is perpendicular to the plane of the spins. This sets the NREE (as shown in Fig. 1d) apart from the usual Rashba EE, whose non-equilibrium spin polarization is on the plane. It also sets the expectation for a large NREE efficiency due to the lack of directional averaging of the spin states contributing to the effect, and the much larger spin-splitting (almost 2 orders of magnitude larger) relative to the relativistic EE [38, 39].

We first demonstrate this physics in a simple 2D generic minimal model that exhibits a  $p$ -wave spin-polarization band structure. We find, even at the simple model level, that the NREE susceptibility of  $p$ -wave magnets surpasses the magnitude calculated for the relativistic Rashba two-dimensional electron gas (2DEG) and recently reported non-relativistic non-coplanar 3Q antiferromagnets (AFMs) with broken TRS [6, 33, 40]. Extending our model analysis to a bi-Kagome lattice geometry, we find a substantial increase in spin-accumulation density. Finally, through first principle calculations, we identify the  $p$ -wave candidate CeNiAsO showing a highly efficient NREE, exhibiting 25 times larger response than the highest Rashba EE [20] and the non-collinear AFM LuFeO<sub>3</sub> [33].

## RESULTS

### Minimal $p$ -wave model

To exemplify the  $p$ -wave electronic structure and its NREE response, we first formulate a low-energy minimal model for the odd-parity magnets based on the simple tight-binding model presented in Fig. 2a. Here the opposite spins are connected by  $[C_{2\perp}||\vec{t}]$  symmetry. The coplanar non-collinear magnetic ordering doubles the unit cell of the square lattice (shown as a dashed green line in Fig. 2a). The electron hopping among the grey nonmagnetic sites is parameterized by  $t$ , and

the  $p$ -wave spin splitting originates from the exchange-dependent hopping parametrized by  $t_J$ . The minimal four-band Hamiltonian is given by [35],

$$H = 2t(\cos\frac{k_x}{2}\tau_1 + \cos k_y) + 2t_J(\sin\frac{k_x}{2}\sigma_1\tau_2 + \cos k_y\sigma_2\tau_3). \quad (1)$$

Pauli matrices  $\sigma$  and  $\tau$  correspond to the spin and site degrees of freedom. The detailed construction of the Hamiltonian is included in SI. Here  $t$ ,  $t_J$  represent the spin-independent and exchange-dependent hopping terms between the nearest neighbor sites within the square lattice geometry.

We illustrate the band structure calculated at  $t_J = 0.25t$  parameter choice of Eq. 1 in Fig. 2b. The fixed energy contour plot at energy  $E = 3.1t$  is plotted in Fig. 2c. As it is clear from the figures, in this low-energy model, the relative displacement of Fermi surfaces of opposite spin, results in a spin-split odd-parity-wave band structure. The band-pairs with opposite out-of-plane spin polarization form a nodal crossing along the  $k_y$  direction. While the direction of the polarization of the states is out of the plane and protected by the spin symmetries of the model, we emphasize that the spin-polarization magnitude of  $p$ -wave magnet is not protected, varying across the Brillouin zone. This  $k$ -dependent spin polarization gradient is essential for the finite NREE in the single-particle models of spin-split bands related by time reversal (see SI for more details).

To compute the non-equilibrium spin density accumulation  $\delta\mathbf{S}$  due to an electric field, we use the Kubo linear response theory as  $\delta S^i = \chi_S^{ij} E^j$ , where  $\mathbf{E}$  is the applied electric field. The spin-current response function has the following expression

$$\chi_S^{ij} = \frac{1}{2\pi} Re \sum_{\mathbf{k}\alpha\beta} S_{\alpha\beta}^i(\mathbf{k}) v_{\beta\alpha}^j(\mathbf{k}) [G_{\mathbf{k}\alpha}^R G_{\mathbf{k}\beta}^A - G_{\mathbf{k}\alpha}^R G_{\mathbf{k}\beta}^R]. \quad (2)$$

Here,  $G_{\mathbf{k}\alpha}^{R(A)} = 1/(\epsilon_F - \epsilon_{\mathbf{k}\alpha} \pm \frac{i\hbar}{2\tau_{\mathbf{k}\alpha}})$  is the retarded (advanced) Green's function evaluated w.r.t the Fermi energy  $\epsilon_F$ .  $\tau_{\mathbf{k}\alpha}$  is the quasiparticle lifetime, taken here to be constant,  $\hbar/\Gamma$ . We can separate the spin density into two parts depending on the contributions from the intra-band,  $\delta S_{\text{intra}}$  and inter-band,  $\delta S_{\text{inter}}$ . The intra-band term with fermi surface contribution has the following expression [41, 42],

$$\delta\mathbf{S}_{\text{intra}} = \frac{e\hbar}{2\Gamma} \int \frac{d^2k}{(2\pi)^2} \sum_{\alpha} \mathbf{S}_{\mathbf{k}\alpha}(\mathbf{E}\cdot\mathbf{v})_{\mathbf{k}\alpha} \delta(E_{\mathbf{k}\alpha} - E_F). \quad (3)$$

The  $\delta\mathbf{S}_{\text{intra}}$  has the dominant contribution to charge spin conversion. The inter-band term can be expressed as,

$$\delta\mathbf{S}_{\text{inter}} = e\hbar \int \frac{d^2k}{(2\pi)^2} \sum_{\alpha\neq\beta} (f_{\mathbf{k}\alpha} - f_{\mathbf{k}\beta}) \text{Im}[\mathbf{S}_{\alpha\beta}(\mathbf{E}\cdot\mathbf{v})_{\beta\alpha}] \times \frac{(E_{\mathbf{k}\alpha} - E_{\mathbf{k}\beta})^2 - \Gamma^2}{[(E_{\mathbf{k}\alpha} - E_{\mathbf{k}\beta})^2 - \Gamma^2]^2}. \quad (4)$$

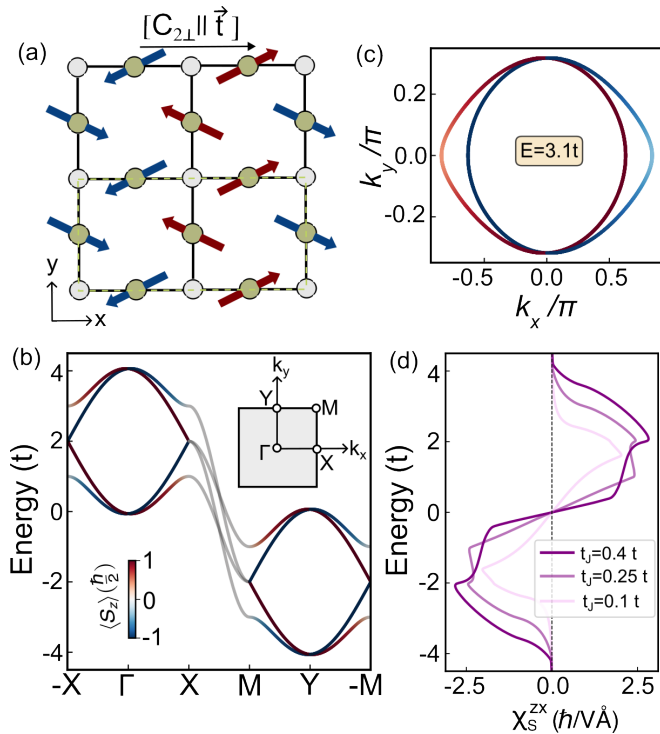


FIG. 2. (a) Schematic of the lattice model with a coplanar non-collinear spin arrangement on the crystal with the spin arrangement that realizes the unconventional p-wave phase. The unit cell is marked with dashed green line. (b) Energy dispersion for  $t_J = 0.25 t$  along high-symmetry momentum paths showing parity broken time-reversal symmetric spin splitting. The color represent the out-of-plane spin component. The opposite spin bands are completely degenerate along the  $k_y$  direction forming a nodal line. (c) Constant energy  $E = 3.1t$  contour with  $t_J = 0.25 t$ . (d) Variation of the NREE response with the strength of the exchange term. An increase of  $t_J$  enhances the shifting of opposite spin bands in opposite momentum directions, therefore, the response strength  $\chi_S$  increases.

Under time reversal symmetry (TRS)  $S \rightarrow -S$  and  $\mathbf{v} \rightarrow -\mathbf{v}$ . Therefore,  $\delta S_{\text{intra}}$  is allowed under TRS. However, the kernel of  $\delta S_{\text{inter}}$  has very similar symmetry properties as the Berry curvature of the system, which vanishes if the system preserves TRS. For this reason, the ‘intra’ and ‘inter’ band components are often referred as  $\mathcal{T}^{\text{even}}$  and  $\mathcal{T}^{\text{odd}}$  part of the Edelstein response tensor. As  $\mathcal{T}^{\text{odd}}$  is the odd Fermi surface property under time-reversal symmetry, it is only allowed for ferromagnets, altermagnets and some non-collinear AFMs breaking TRS [33, 43] but prohibited in the  $p$ -wave candidates, as we also verify in our numerical calculations. For the identified  $p$ -wave material candidates in Ref. [35] from the materials listed in MAGNDATA [44], we have included the symmetry-allowed tensorial form of the susceptibility in Table-I of SI.

For our minimal model Hamiltonian, the  $\chi_S^{zx}$  is the only finite component of the symmetry-constrained rank-

2 tensor (Fig. 2d). The maximum value of the  $\chi_S$  increases with  $t_J$  due to the increasing anisotropy between the spin channels. The particle-hole symmetry evidenced in the response (Fig. 2d) is in agreement with the model band structure shown in Fig. 2b. In order to compare to other systems, we look at  $\chi_S$  within (i) a non-coplanar AFM model with broken TRS with 3Q spin-texture [33] and (ii) a two-dimensional electron gas (2DEG) with relativistic Rashba SOC. For the former case, the non-equilibrium susceptibility, integrated over the unit cell, is reported to be  $\chi_S^{3Q-AFM} \sim 0.5\hbar\text{\AA}/V$  [33]. The non-equilibrium spin density for the Rashba 2DEG is given by  $\delta S^R/eE = \alpha_R m_0/\hbar^2\pi\Gamma$  [6]. We set  $\Gamma = 0.1$  eV,  $\alpha_R = 10^{-9}$  eVm as the typical Rashba strength expected in transition metal heterostructures [40, 45], with  $m_0$  being the free electron mass. This gives an effective Edelstein response  $\chi_S^R \sim 0.04\hbar/V\text{\AA}$ . Already at the simple model level, the strength of  $\chi_S$  of the minimal  $p$ -wave model is 1-2 orders larger than that of the reported non-relativistic non-coplanar 3Q-AFM and relativistic Rashba 2DEG model.

### Tight Binding model of $p$ -wave bi-kagome magnet

We next analyze the NREE in  $p$ -wave magnets within a multi-orbital two-dimensional Kagome lattice, as described by the Hamiltonian,

$$H = \sum_i \mathcal{J}_i \cdot \boldsymbol{\sigma} c_i^\dagger c_i + t_h \sum_{\langle ij \rangle} c_i^\dagger c_j. \quad (5)$$

Here,  $c^\dagger$  and  $c$  are the fermionic creation and annihilation operators.  $i, j$  are the site indices. The first term in eq. 5 represents the interaction term where  $\mathcal{J}_i$  as the local exchange parameter.  $\boldsymbol{\sigma}$  is the vector containing three spin Pauli matrices. The kinetic energy of the Hamiltonian is included in the second term, where  $t_h$  is the isotropic nearest neighbor hopping strength. We choose the spin direction for six-inequivalent sites to be  $\hat{\mathcal{J}}_1 = -\hat{\mathcal{J}}_4 = (\cos\theta_s \hat{x} + \sin\theta_s \hat{y})$ ,  $\hat{\mathcal{J}}_2 = -\hat{\mathcal{J}}_5 = (-\cos\theta_s \hat{x} + \sin\theta_s \hat{y})$ ,  $\hat{\mathcal{J}}_3 = -\hat{\mathcal{J}}_6 = -\hat{y}$  with  $\theta_s = \frac{\pi}{6}$ . The coplanar noncollinear magnetic ordering shown in Fig. 3a fulfils the spin symmetry criteria for collinear  $p$ -wave spin-polarization band structure presented earlier. The neighboring red and blue triangular sub-units containing opposite  $\Gamma_{4g}$  phases [46], are connected by  $\mathcal{T}\vec{t}$  symmetry as shown by the black arrow. Although the  $120^\circ$  spin-order preserves the parity for a single Kagome unit cell, the  $\mathcal{T}\vec{t}$  symmetric spin-order on the Kagome lattice breaks the inversion. As already emphasized before, due to the  $[C_{2\perp}||\vec{t}]$  spin symmetry, the in-plane  $S_x$  and  $S_y$  components of the spins are identically zero for every momentum. The  $\langle S_z \rangle$  polarized band structure along the high-symmetry  $-M-\Gamma-M$  direction is shown in Fig. 3b. Here we choose  $|\mathcal{J}| = |t_h| = 1.0$  eV throughout our model calculations.

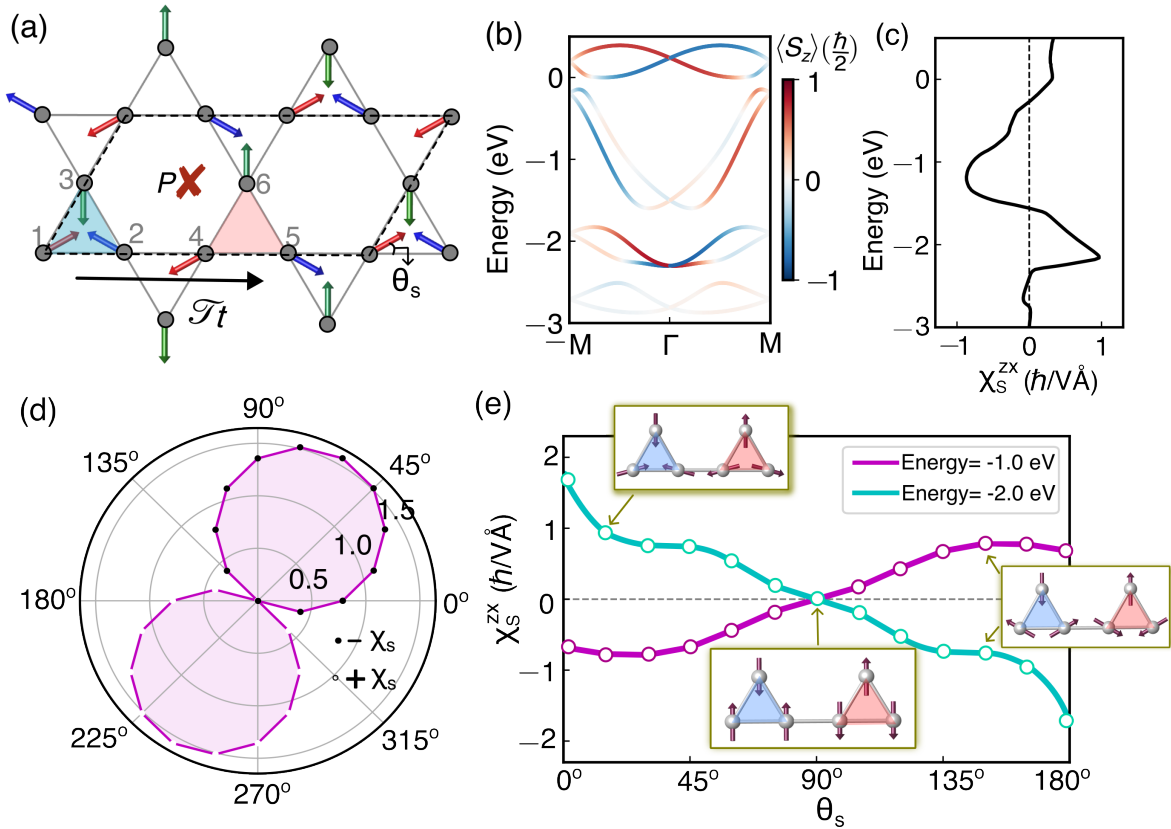


FIG. 3. (a) Direct space magnetic order of the Kagome lattice with twice propagation along the  $x$ -axis. The magnetic order breaks the inversion and exhibits combined TRS and lattice translation symmetry,  $\mathcal{T}\hat{t}$  marked by the black arrow, which connects the spins in the blue and red shaded triangles. The coplanar spins in each magnetic triangle observe  $120^\circ$  spin alignment. The spin canting angle of the red spin,  $\theta_s$ , is also marked. (b) The out-of-plane spin-projected band dispersion along  $-M-\Gamma-M$  high-symmetry direction. (c) The non-equilibrium intra-band susceptibility density,  $\chi_S^{zx}$ , for electric field  $\mathbf{E} = E\hat{x}$ . (d) The angular distribution of  $\chi_S^{zx}$  (in units of  $\hbar/V\text{\AA}$ ) for energy -0.1 eV w.r.t the electric field direction. The white and black circles represent the positive and negative sign of  $\chi_S$  (e). The magnitude of  $\chi_S^{zx}$  gradually increases with the spin canting angle  $\theta_s$ , relative to the collinear arrangement at  $\theta_s = 90^\circ$ .

Our calculations reveal a significant NREE for the Kagome TB model. We plot the  $\chi_S$  response choosing the direction of the applied electric field along  $x$  with  $\Gamma = 0.01$  eV in Fig. 3c. The strength of the NREE susceptibility is of the same order as in the minimal  $p$ -wave model. We also show in Fig. 3d the expected  $p$ -wave anisotropy in the directional dependence of  $\chi_S$ , by rotating the  $\vec{E}$  in the  $x-y$  plane and plotting the  $\chi_S$  for a fixed energy  $E - E_F = -0.1$  eV in Fig. 3d. The black and white circles represent the positive and negative signs of the NREE susceptibility. The  $\chi_S$  shows a nodal line for  $\mathbf{E} \parallel (-\frac{\sqrt{3}}{2}\hat{x} + \frac{1}{2}\hat{y})$  independent of the chemical potential. Hence, the angular measurement of the NREE provides a strong measurable signature for this NREE in these  $p$ -wave magnets.

We next explore the NREE dependence on the chirality of spins within the Kagome lattice, by adjusting the canting angle between the spins  $\theta$  (inset of Fig. 3a and e). As a result, the  $C_3$  symmetry of neighboring spins

within individual triangles is disrupted, while the overall  $[C_2 \parallel \vec{t}]$  connecting the red and blue triangles is preserved. The change in spin canting configuration changes the  $\chi_S$  anisotropy pattern from that of the  $120^\circ$  order (see SI for more details). For  $\theta_s = 90^\circ$ ,  $\chi_S$  vanishes since the spin-order becomes collinear promoting spin degenerate bands, consistent with the result from the full classification and delimitation of collinear spin arrangements on lattices by the spin symmetries [36]. In Fig. 3e we have plotted the NREE for two different energy values for  $\theta_s$  in the range of  $0^\circ - 180^\circ$ . The increase in canting angle relative to the collinear arrangement ( $\theta_s = 90^\circ$ ) enhances the NREE and changes sign at  $\theta_s = 90^\circ$ .

#### Material Candidate: CeNiAsO

We next compute the NREE for the realistic  $p$ -wave magnetic material candidate CeNiAsO [35]. The sys-



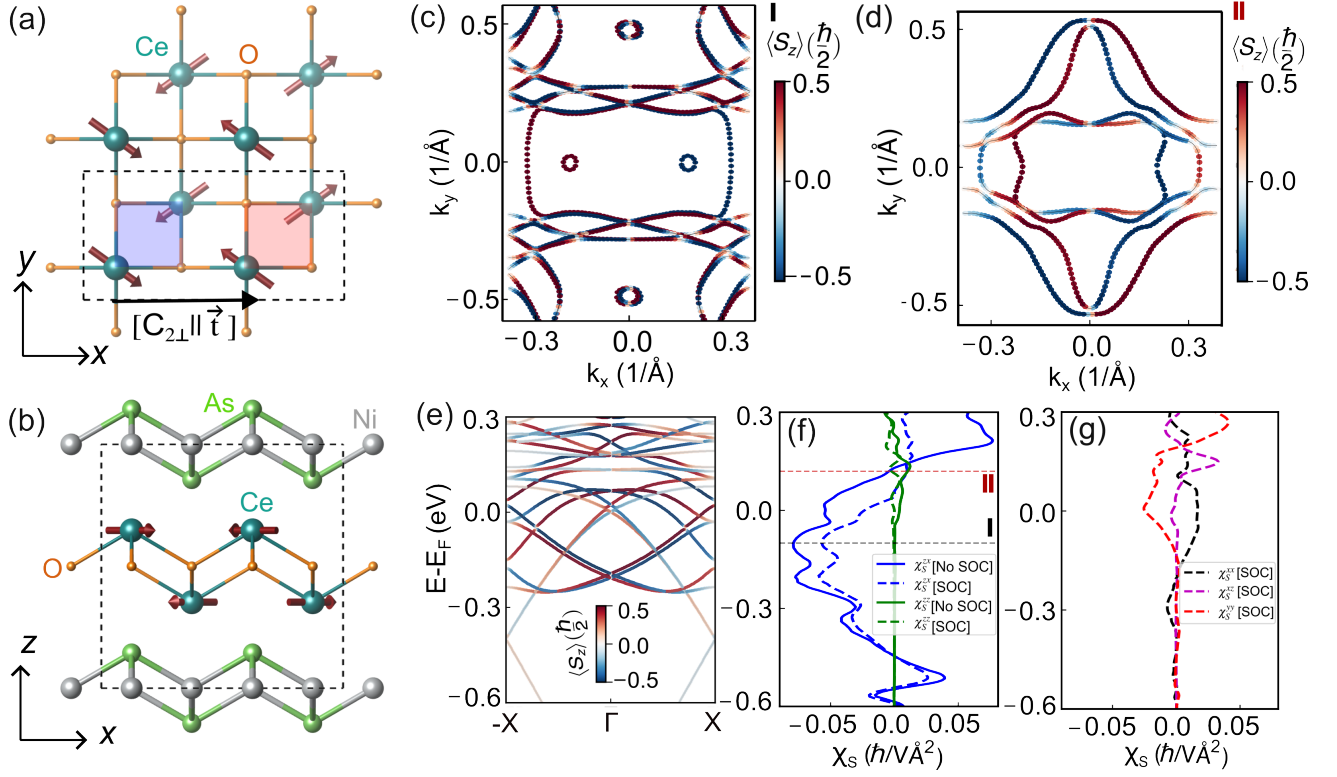


FIG. 4. Top (a) and side (b) view of the unit cell of CeNiAsO crystal and the co-planar magnetic order with  $\mathcal{T}t$  symmetry. The out-of-plane spin projected constant energy isosurface at  $E \sim -0.1$  eV (c) and  $E \sim 0.12$  eV (d) in the  $k_z = 0$  momentum plane. (e) Nonrelativistic odd-parity wave spin splitting of energy bands plotted along the  $-X-\Gamma-X$  path. The colormap represents the out-of-plane  $\langle S_z \rangle$  component. (f) The symmetry-allowed components of non-equilibrium intra-band susceptibility density,  $\chi_S^{zx}$  and  $\chi_S^{zz}$ . The modifications of the specific components in the presence of SOC are shown in dashed curves. The isoenergy cuts of (c) and (d) are at the energy where the  $\chi_S^{zx}$  component of the NREE susceptibility acquires maximum and minimum values as indicated by dotted lines in (f). (g) Susceptibility components arise due to the sole relativistic effect. SOC leads to finite  $\chi_S^{xx}$ ,  $\chi_S^{zz}$  and  $\chi_S^{yy}$  which are not allowed within the NREE susceptibility tensor.

tem shows a co-planar commensurate magnetic order with a moment  $0.37 \mu_B$  below Néel temperature,  $T_N = 7.6\text{K}$  [47]. From the spin symmetry analysis, the experimentally reported coplanar non-collinear magnetic order of CeNiAsO, as shown in Fig. 4a and 4b, implies the coplanar spin only group symmetry  $\mathbf{r}_s = \{E, \bar{C}_{2z}\}$ , where  $\bar{C}_{2z}$  is  $180^\circ$  rotation around  $z$ -axis combined with spin-space inversion (time reversal). The nontrivial spin-space group  $\mathbf{G}^S$  in CeNiAsO contains the following symmetry elements [35, 48, 49]:  $[E||E]$ ,  $[E||\mathcal{M}_y \vec{t}_{\frac{b}{2}}]$ ,  $[C_{2z}||\vec{t}_{\frac{a}{2}}]$ ,  $[C_{2z}||\mathcal{M}_y \vec{t}_{(\frac{a}{2} + \frac{b}{2})}]$ ,  $[C_{2x}||C_{2y} \vec{t}_{\frac{b}{2}}]$ ,  $[C_{2y}||C_{2y} \vec{t}_{(\frac{a}{2} + \frac{b}{2})}]$ ,  $[C_{2x}||P]$ ,  $[C_{2y}||P \vec{t}_{\frac{a}{2}}]$ , where  $C$ , and  $\mathcal{M}$  denote rotation and mirror operations, and  $\vec{t}_i$  is the translation along  $i$  of the lattice vector. The symmetry operation  $[C_{2z}||\vec{t}_{\frac{a}{2}}]$  (see Fig. 4a) in combination with broken inversion symmetry fulfils the above symmetry conditions for the odd-parity-wave magnetic state. Additionally, the symmetry  $[C_{2y}||C_{2y}]$  enforces a single spin-unpolarized line  $k_x = k_z = 0$  in the  $k_z = 0$  plane, implying  $E(k_x, k_y, k_z, \sigma_z) = E(-k_x, k_y, -k_z, -\sigma_z)$ . We plot

the band dispersion of CeNiAsO in Fig. 4e. The bands have opposite out-of-plane spin polarization  $S_z$  for opposite momentum with a linear crossing at the  $\Gamma$  point. The fixed energy contour at  $E - E_F = -0.1$  eV and at  $+0.12$  eV within  $k_x - k_y$  plane (Fig. 4c, 4d) shows a nodal line along  $k_y$  direction.

We compute all the components of the NREE susceptibility for metallic CeNiAsO in the limit of zero SOC, shown by solid lines in Fig. 4f. Our spin symmetry analysis (see SI for details) yields that only the  $\chi_S^{zx}$  and  $\chi_S^{zz}$  components survive, which is consistent with our numerical results. Given the negligible van-der-Waals interaction between the Ce layers stacked along the  $z$ -axis within the bulk geometry, we find a small  $v_z$  component of the velocity. Therefore the obtained  $\chi_S^{zz}$  value is substantially lower than that of  $\chi_S^{zx}$ . Fig. 4c and 4d represent the isoenergy contours at energies where the NREE susceptibility  $\chi_S^{zx}$  reaches the maximum and minimum values, as shown with dotted lines in Fig. 4f.

Of course, along with non-relativistic exchange-driven effects, SOC can also have an impact due to the fact that

Ce is a rare-earth element. Within the relevant magnetic point group analysis, by its own construction, the spin group symmetry [ $C_{2\perp}||\vec{t}$ ] is broken by spin-orbit coupling and, therefore, no longer enforces the polarization direction to be out of the plane. The induced finite in-plane spin components hence emerge solely due to SOC effect. In Fig. 4f, we show the change of the NREE susceptibility non-zero components in the presence of SOC with dashed curves. The susceptibility components emerging solely from the relativistic origin are plotted in Fig. 4g. The details of relativistic band dispersion and the corresponding tensorial form of the non-equilibrium spin accumulation susceptibility are included in section 5 of SI. While the NREE dominates prominently over a large range of energies, the contributions of the SOC susceptibilities of in-plane polarization can be exploited to calibrate the relevance of this contribution in general. Comparing the relative magnitude of the in-plane and out-of-plane EE susceptibilities should be a good experimental test of the relevance of the NREE.

Next, we compare the magnitude of NREE susceptibility of  $\mathcal{T}\vec{t}$  symmetric  $p$ -wave magnets with recently reported non-relativistic spin accumulation within non-collinear magnets with broken TRS, i.e. non  $p$ -wave magnets. The NREE reported for non-centrosymmetric  $\text{LuFeO}_3$  is  $0.5 \text{ } \hbar\text{\AA}/V$  calculated within unit cell of volume  $360.61 \text{ \AA}^3$  [33]. The effective  $\chi_S^{zx}$  integrated over the unit cell of volume  $267.50 \text{ \AA}^3$  of  $\text{CeNiAsO}$  gives NREE  $\sim 13 \text{ } \hbar\text{\AA}/V$ , which is 25 times higher in magnitude than that of NREE reported for  $\text{LuFeO}_3$ .

## DISCUSSION AND OUTLOOK

We predict here a highly efficient NREE in  $p$ -wave magnets. This type of coplanar noncollinear magnetic order preserves TRS in momentum space (through the  $\mathcal{T}\vec{t}$  symmetry) while exhibiting  $p$ -parity polarized band structure [35]. Their spin symmetry [ $C_{2\perp}||\vec{t}$ ] forces the polarization direction in the band structure to be perpendicular to the plane of spin coplanarity. This unique feature of  $p$ -wave magnets gives them an anisotropic EE signature relative to their relativistic and other magnetic system counterparts and can lead to unprecedented high efficiency in spin-to-charge conversion. The non-equilibrium spin accumulation within  $p$ -wave magnets does not originate from the SOC effect but rather from the exchange interaction of the non-collinear magnetic order. The inevitable presence of SOC can lead to contributions to the EE within these materials, particularly in the presence of heavy elements, and its contribution to the spin-charge conversion efficiency can be estimated by the measured in-plane vs. out-of-plane susceptibilities. However, this contribution is expected to be significantly less pronounced in material candidates with

lighter elements. We predict here that the charge-to-spin conversion in the metallic material candidate  $\text{CeNiAsO}$ , showing coplanar noncollinear magnetic order, should be dominated by the NREE. The NREE in  $p$ -wave magnet suggests the possibility of current-driven controlled spin dynamics, which is fundamentally different from the relativistic effects observed in conventional spin-transfer and spin-orbit torque devices.

## METHODS

We have used density functional theory (DFT) in the plane wave basis set. We used the Perdew-Burke-Ernzerhof (PBE) [50] implementation of the generalized gradient approximation (GGA) for the exchange-correlation. This was combined with the projector augmented wave potentials [51, 52] as implemented in the Vienna *ab initio* simulation package (VASP) [53, 54]. The kinetic energy cutoff of the plane wave basis for the DFT calculations was chosen to be 460 eV. A  $\Gamma$ -centered  $4\times 8\times 4$   $k$ -point grids are used to perform the momentum-space calculations for the Brillouin zone (BZ) integration. We have constrained the magnetic moments without incorporating SOC and switching off the crystal symmetry to capture the sole non-relativistic effect. A penalty contribution to the total energy is considered in these calculations to constrain the moments. The penalty energy fixes the local moment into a specific direction [53, 54]

$$E = E_0 + \sum \gamma [\vec{M}_i - \hat{M}_i^0 (\hat{M}_i^0 \cdot \vec{M}_i)]^2, \quad (6)$$

where  $E_0$  is the DFT energy without any constraint, and the second term represents the penalty energy contribution due to non-collinear direction constraint.  $\hat{M}_i^0$  and  $\vec{M}_i$  represent the unit vector along the desired direction of magnetic moment and integrated magnetic moment inside the Wigner-Seitz cell at site  $i$ , respectively. The sizes of the Wigner size radii are to be chosen as 1.98  $\text{\AA}$ , 1.21  $\text{\AA}$ , 1.09  $\text{\AA}$  and 0.24  $\text{\AA}$  for Ce, Ni, As and O atoms, respectively. The choice of  $\gamma$  controls the penalty energy contribution. In our calculations for  $\text{CeNiAsO}$ , we set  $\gamma = 6 \text{ eV}/\mu_B^2$  to get negligible penalty contribution  $1\times 10^{-8} \text{ eV}$ . We construct the tight-binding model Hamiltonian of  $\text{CeNiAsO}$  by using atom-centred Wannier functions within the VASP2WANNIER90 [55] codes. Utilizing the obtained tight-binding model, we calculate the Edelstein response tensor.

## ACKNOWLEDGEMENT

JS, AC, ABH, and LS acknowledge funding by the Deutsche Forschungsgemeinschaft (DFG, German Research Foundation) - TRR 173 - 268565370 (project A03) and TRR 288 - 422213477 (project A09 and B05),

and the Alexander von Humboldt Foundation. TJ acknowledges support by the Ministry of Education of the Czech Republic CZ.02.01.01/00/22008/0004594 and, ERC Advanced Grant no. 101095925. We acknowledge the high-performance computational facility of supercomputer ‘Mogon’ at Johannes Gutenberg Universität Mainz, Germany. The authors acknowledge fruitful discussions with Gerrit Bauer, Rafael González Hernández, and Nayra A Alvarez Pari.

\* [atasi.chakraborty@uni-mainz.de](mailto:atasi.chakraborty@uni-mainz.de)

† [sinova@uni-mainz.de](mailto:sinova@uni-mainz.de)

- [1] I. Žutić, J. Fabian, and S. Das Sarma, Spintronics: Fundamentals and applications, *Rev. Mod. Phys.* **76**, 323 (2004), [arXiv:0405528 \[cond-mat\]](https://arxiv.org/abs/0405528).
- [2] S. Maekawa, Concepts in Spin Electronics, *Concepts Spin Electron.* **9780198568**, 1 (2007).
- [3] J. Sinova, S. O. Valenzuela, J. Wunderlich, C. H. Back, and T. Jungwirth, Spin Hall effects, *Rev. Mod. Phys.* **87**, 1213 (2015).
- [4] A. Manchon, J. Železný, I. M. Miron, T. Jungwirth, J. Sinova, A. Thiaville, K. Garello, and P. Gambardella, Current-induced spin-orbit torques in ferromagnetic and antiferromagnetic systems, *Rev. Mod. Phys.* **91**, 035004 (2019), [arXiv:1801.09636](https://arxiv.org/abs/1801.09636).
- [5] a. G. Aronov and Y. B. Lyanda-Geller, Nuclear electric resonance and orientation of carrier spins by an electric field, *JETP Lett.* **50**, 431 (1989).
- [6] V. M. Edelstein, Spin polarization of conduction electrons induced by electric current in two-dimensional asymmetric electron systems, *Solid State Commun.* **73**, 233 (1990).
- [7] P. Gambardella and I. M. Miron, Current-induced spin-orbit torques, *Philos. Trans. R. Soc. A Math. Phys. Eng. Sci.* **369**, 3175 (2011).
- [8] E. Lesne, Y. Fu, S. Oyarzun, J. C. Rojas-Sánchez, D. C. Vaz, H. Naganuma, G. Sicoli, J.-P. Attané, M. Jamet, E. Jacquet, J.-M. George, A. Barthélémy, H. Jaffrès, A. Fert, M. Bibes, and L. Vila, Highly efficient and tunable spin-to-charge conversion through Rashba coupling at oxide interfaces, *Nat. Mater.* **15**, 1261 (2016).
- [9] D. C. Vaz, P. Noël, A. Johansson, B. Göbel, F. Y. Bruno, G. Singh, S. McKeown-Walker, F. Trier, L. M. Vicente-Arche, A. Sander, S. Valencia, P. Bruneel, M. Vivek, M. Gabay, N. Bergeal, F. Baumberger, H. Okuno, A. Barthélémy, A. Fert, L. Vila, I. Mertig, J. P. Attané, and M. Bibes, Mapping spin-charge conversion to the band structure in a topological oxide two-dimensional electron gas, *Nat. Mater.* **18**, 1187 (2019).
- [10] S. Manipatruni, D. E. Nikonov, C. C. Lin, T. A. Gosavi, H. Liu, B. Prasad, Y. L. Huang, E. Bonturim, R. Ramesh, and I. A. Young, Scalable energy-efficient magnetoelectric spin-orbit logic, *Nature* **565**, 35 (2019).
- [11] J. Železný, H. Gao, K. Výborný, J. Zemen, J. Mašek, A. Manchon, J. Wunderlich, J. Sinova, and T. Jungwirth, Relativistic Néel-order fields induced by electrical current in antiferromagnets, *Phys. Rev. Lett.* **113**, 157201 (2014), [arXiv:1410.8296](https://arxiv.org/abs/1410.8296).
- [12] B. A. Bernevig and S. C. Zhang, Intrinsic spin hall effect in the two-dimensional hole gas, *Phys. Rev. Lett.* **95**, 016801 (2005), [arXiv:0411457 \[cond-mat\]](https://arxiv.org/abs/0411457).
- [13] A. Manchon and S. Zhang, Theory of nonequilibrium intrinsic spin torque in a single nanomagnet, *Phys. Rev. B* **78**, 212405 (2008).
- [14] A. Manchon and S. Zhang, Theory of spin torque due to spin-orbit coupling, *Phys. Rev. B* **79**, 094422 (2009).
- [15] A. Matos-Abiague and R. L. Rodríguez-Suárez, Spin-orbit coupling mediated spin torque in a single ferromagnetic layer, *Phys. Rev. B* **80**, 94424 (2009).
- [16] A. Chernyshov, M. Overby, X. Liu, J. K. Furdyna, Y. Lyanda-Geller, and L. P. Rokhinson, Evidence for reversible control of magnetization in a ferromagnetic material by means of spin-orbit magnetic field, *Nat. Phys.* **5**, 656 (2009), [arXiv:0812.3160](https://arxiv.org/abs/0812.3160).
- [17] I. Garate and A. H. MacDonald, Influence of a transport current on magnetic anisotropy in gyrotropic ferromagnets, *Phys. Rev. B* **80**, 134403 (2009), [arXiv:0905.3856](https://arxiv.org/abs/0905.3856).
- [18] V. V. Bryksin and P. Kleinert, Theory of electric-field-induced spin accumulation and spin current in the two-dimensional Rashba model, *Phys. Rev. B - Condens. Matter Mater. Phys.* **73**, 1 (2006).
- [19] S. Leiva-Montecinos, J. Henk, I. Mertig, and A. Johansson, Spin and orbital Edelstein effect in a bilayer system with Rashba interaction, *Phys. Rev. Res.* **5**, 1 (2023), [arXiv:2307.02872](https://arxiv.org/abs/2307.02872).
- [20] J. C. Rojas-Sánchez, S. Oyarzún, Y. Fu, A. Marty, C. Vergnaud, S. Gambarelli, L. Vila, M. Jamet, Y. Ohtsubo, A. Taleb-Ibrahimi, P. Le Fèvre, F. Bertran, N. Reyren, J. M. George, and A. Fert, Spin to Charge Conversion at Room Temperature by Spin Pumping into a New Type of Topological Insulator:  $\alpha$ -Sn Films, *Phys. Rev. Lett.* **116**, 096602 (2016), [arXiv:1509.02973](https://arxiv.org/abs/1509.02973).
- [21] Y. Kato, R. C. Myers, A. C. Gossard, and D. D. Awschalom, Coherent spin manipulation without magnetic fields in strained semiconductors, *Nature* **427**, 50 (2004), [arXiv:mglazov.110mb.com/bibliography/kato04b.pdf \[http:\]](https://arxiv.org/abs/mglazov.110mb.com/bibliography/kato04b.pdf).
- [22] R. Peters and Y. Yanase, Strong enhancement of the Edelstein effect in f-electron systems, *Phys. Rev. B* **97**, 115128 (2018), [arXiv:1803.05092](https://arxiv.org/abs/1803.05092).
- [23] A. Johansson, J. Henk, and I. Mertig, Edelstein effect in Weyl semimetals, *Phys. Rev. B* **97**, 1 (2018).
- [24] S.-H. Yang, R. Naaman, Y. Paltiel, and S. S. P. Parkin, Chiral spintronics, *Nat. Rev. Phys.* **3**, 328 (2021).
- [25] J. C. Sánchez, L. Vila, G. Desfonds, S. Gambarelli, J. P. Attané, J. M. De Teresa, C. Magén, and A. Fert, Spin-to-charge conversion using Rashba coupling at the interface between non-magnetic materials, *Nat. Commun.* **4**, 2944 (2013).
- [26] Q. Shao, G. Yu, Y. W. Lan, Y. Shi, M. Y. Li, C. Zheng, X. Zhu, L. J. Li, P. K. Amiri, and K. L. Wang, Strong Rashba-Edelstein Effect-Induced Spin-Orbit Torques in Monolayer Transition Metal Dichalcogenide/Ferromagnet Bilayers, *Nano Lett.* **16**, 7514 (2016).
- [27] M. Trama, I. Gaiardoni, C. Guarcello, J. I. Facio, A. Maiellaro, F. Romeo, R. Citro, and J. van den Brink, Non-linear anomalous Edelstein response at alternating magnetic interfaces, *,* **1** (2024), [arXiv:2410.18036](https://arxiv.org/abs/2410.18036).
- [28] G. Lazrak, B. Göbel, A. Barthélémy, I. Mertig, A. Johansson, and M. Bibes, Boosting the Edelstein ef-

- fect of two-dimensional electron gases by ferromagnetic exchange, *Phys. Rev. Res.* **6**, 23074 (2023), [arXiv:2310.03348](#).
- [29] A. Johansson, B. Göbel, J. Henk, M. Bibes, and I. Mertig, Spin and orbital Edelstein effects in a two-dimensional electron gas: Theory and application to SrTiO<sub>3</sub> interfaces, *Phys. Rev. Res.* **3**, 13275 (2021).
- [30] L. Chirolli, M. T. Mercaldo, C. Guarcello, F. Giazotto, and M. Cuoco, Colossal Orbital Edelstein Effect in Non-centrosymmetric Superconductors, *Phys. Rev. Lett.* **128**, 217703 (2022), [arXiv:2107.07476](#).
- [31] S. Hayami, Y. Yanagi, and H. Kusunose, Spontaneous antisymmetric spin splitting in noncollinear antiferromagnets without spin-orbit coupling, *Phys. Rev. B* **101**, 220403 (2020), [arXiv:2001.05630](#).
- [32] M. Naka, S. Hayami, H. Kusunose, Y. Yanagi, Y. Motome, and H. Seo, Spin current generation in organic antiferromagnets, *Nat. Commun.* **10**, 4305 (2019), [arXiv:1902.02506](#).
- [33] R. González-Hernández, P. Ritzinger, K. Výborný, J. Železný, and A. Manchon, Non-relativistic torque and Edelstein effect in non-collinear magnets, *Nat. Commun.* **15**, 7663 (2024), [arXiv:2310.06499](#).
- [34] M. Hu, O. Janson, C. Felser, P. McClarty, J. van den Brink, and M. G. Vergniory, Spin Hall and Edelstein Effects in Novel Chiral Noncollinear Altermagnets, *arXiv*, **1** (2024), [arXiv:2410.17993](#).
- [35] A. B. Hellenes, T. Jungwirth, R. Jaeschke-Ubiergo, A. Chakraborty, J. Sinova, and L. Šmejkal, P-wave magnets, *Arxiv Prepr.* (2023), [arXiv:2309.01607](#).
- [36] L. Šmejkal, J. Sinova, and T. Jungwirth, Beyond Conventional Ferromagnetism and Antiferromagnetism: A Phase with Nonrelativistic Spin and Crystal Rotation Symmetry, *Phys. Rev. X* **12**, 031042 (2022), [arXiv:2105.05820](#).
- [37] L. Šmejkal, J. Sinova, and T. Jungwirth, Emerging Research Landscape of Altermagnetism, *Phys. Rev. X* **12**, 040501 (2022), [arXiv:2204.10844](#).
- [38] K. Ishizaka, M. S. Bahramy, H. Murakawa, M. Sakano, T. Shimojima, T. Sonobe, K. Koizumi, S. Shin, H. Miyahara, A. Kimura, K. Miyamoto, T. Okuda, H. Namatame, M. Taniguchi, R. Arita, N. Nagaosa, K. Kobayashi, Y. Murakami, R. Kumai, Y. Kaneko, Y. Onose, and Y. Tokura, Giant Rashba-type spin splitting in bulk BiTeI, *Nat. Mater.* **10**, 521 (2011).
- [39] M. S. Bahramy, R. Arita, and N. Nagaosa, Origin of giant bulk Rashba splitting: Application to BiTeI, *Phys. Rev. B - Condens. Matter Mater. Phys.* **84**, 2 (2011), [arXiv:1105.2757](#).
- [40] A. Johansson, J. Henk, and I. Mertig, Theoretical aspects of the Edelstein effect for anisotropic two-dimensional electron gas and topological insulators, *Phys. Rev. B* **93**, 1 (2016).
- [41] I. Garate, K. Gilmore, M. D. Stiles, and A. H. MacDonald, Nonadiabatic spin-transfer torque in real materials, *Phys. Rev. B* **79**, 104416 (2009).
- [42] J. Železný, H. Gao, K. Výborný, J. Zemen, J. Mašek, A. Manchon, J. Wunderlich, J. Sinova, and T. Jungwirth, Relativistic Néel-order fields induced by electrical current in antiferromagnets, *Phys. Rev. Lett.* **113**, 1 (2014), [arXiv:1410.8296](#).
- [43] G. Gurung, D. F. Shao, and E. Y. Tsymbal, Transport spin polarization of noncollinear antiferromagnetic antiperovskites, *Phys. Rev. Mater.* **5**, 1 (2021), [arXiv:2108.09540](#).
- [44] S. V. Gallego, J. Manuel Perez-Mato, L. Elcoro, E. S. Tasci, R. M. Hanson, M. I. Aroyo, G. Madariaga, J. M. Perez-Mato, L. Elcoro, E. S. Tasci, R. M. Hanson, M. I. Aroyo, and G. Madariaga, MAGNDATA : towards a database of magnetic structures. II. The incommensurate case, *J. Appl. Cryst.* **49**, 1941 (2016).
- [45] A. Manchon, H. C. Koo, J. Nitta, S. M. Frolov, and R. A. Duine, New perspectives for Rashba spin-orbit coupling, *Nat. Mater.* **14**, 871 (2015), [arXiv:1507.02408](#).
- [46] G. Gurung, D.-F. F. Shao, and E. Y. Tsymbal, Transport spin polarization of noncollinear antiferromagnetic antiperovskites, *Phys. Rev. Mater.* **5**, 124411 (2021), [arXiv:2108.09540](#).
- [47] S. Wu, W. A. Phelan, L. Liu, J. R. Morey, J. A. Tuttmaher, J. C. Neufeind, A. Huq, M. B. Stone, M. Feyngenson, D. W. Tam, B. A. Frandsen, B. Trump, C. Wan, S. R. Dunsiger, T. M. McQueen, Y. J. Uemura, and C. L. Broholm, Incommensurate Magnetism Near Quantum Criticality in CeNiAsO, *Phys. Rev. Lett.* **122**, 197203 (2019), [arXiv:1707.09645](#).
- [48] A. Smolyanyuk, L. Šmejkal, and I. I. Mazin, A tool to check whether a symmetry-compensated collinear magnetic material is antiferro- or altermagnetic, *SciPost Phys. Codebases* **30**, 1 (2024), [arXiv:2401.08784](#).
- [49] K. Shinohara, A. Togo, H. Watanabe, T. Nomoto, I. Tanaka, and R. Arita, Algorithm for spin symmetry operation search, *Acta Crystallogr. Sect. A Found. Adv.* **80**, 94 (2024).
- [50] J. P. Perdew, K. Burke, and M. Ernzerhof, Generalized Gradient Approximation Made Simple, *Phys. Rev. Lett.* **77**, 3865 (1996), [arXiv:0927-0256\(96\)00008](#) [10.1016].
- [51] P. E. Blöchl, Projector augmented-wave method, *Phys. Rev. B* **50**, 17953 (1994), [arXiv:arXiv:1408.4701v2](#).
- [52] G. Kresse and D. Joubert, From ultrasoft pseudopotentials to the projector augmented-wave method, *Phys. Rev. B* **59**, 1758 (1999), [arXiv:0927-0256\(96\)00008](#) [10.1016].
- [53] G. Kresse and J. Hafner, Ab initio molecular dynamics for liquid metals, *Phys. Rev. B* **47**, 558 (1993), [arXiv:0927-0256\(96\)00008](#) [10.1016].
- [54] G. Kresse and J. Furthmüller, Efficient iterative schemes for ab initio total-energy calculations using a plane-wave basis set, *Phys. Rev. B* **54**, 11169 (1996), [arXiv:0927-0256\(96\)00008](#) [10.1016].
- [55] I. Souza, N. Marzari, and D. Vanderbilt, Maximally localized Wannier functions for entangled energy bands, *Phys. Rev. B* **65**, 035109 (2001), [arXiv:0108084](#) [cond-mat].